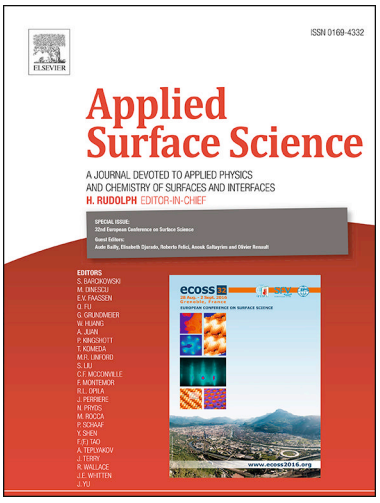

Full Length Article

Chitosan-58S bioactive glass nanocomposite coatings on TiO_2 nanotube: Structural and biological properties

Hamidreza Mokhtari, Zahra Ghasemi, Mahshid Kharaziha, Fathollah Karimzadeh, Farzaneh Alihosseini

PII: S0169-4332(18)30336-2
DOI: https://doi.org/10.1016/j.apsusc.2018.01.314
Reference: APSUSC 38453

To appear in: *Applied Surface Science*

Received Date: 11 September 2017
Revised Date: 10 January 2018
Accepted Date: 31 January 2018

Please cite this article as: H. Mokhtari, Z. Ghasemi, M. Kharaziha, F. Karimzadeh, F. Alihosseini, Chitosan-58S bioactive glass nanocomposite coatings on TiO_2 nanotube: Structural and biological properties, *Applied Surface Science* (2018), doi: https://doi.org/10.1016/j.apsusc.2018.01.314

Chitosan-58S bioactive glass nanocomposite coatings on TiO_2 nanotube: Structural and biological properties

Hamidreza Mokhtari[1], Zahra Ghasemi[1], Mahshid Kharaziha[1*], Fathollah Karimzadeh[1], Farzaneh Alihosseini[2]

1. Department of Materials Engineering, Isfahan University of Technology, Isfahan 84156-83111, Iran

2. Department of Textile Engineering, Isfahan University of Technology, Isfahan 84156-83111, Iran

* Corresponding author e-mail: kharaziha@cc.iut.ac.ir

Abstract

Bacterial infection and insignificant osseointegration have been recognized as the main reasons of the failures of titanium based implants. The aim of this study was to apply titanium oxide nanotube (TNT) array coating on titanium using electrochemical anodization process as a more appropriate substrate for the chitosan-58S bioactive glass nanocomposite coatings covered TNTs through a conventional dip-coating process. Results showed that a TNT layer with average inner diameter of 82 ± 19 nm and wall's thickness of 23 ± 9 nm was developed on titanium surface using electrochemical anodization process. Roughness and contact angle measurement showed that TNT with R_a= 449 nm had highest roughness and hydrophilicity which then reduced to 86 nm and 143 nm for TNT/Chitosan and TNT/58S-BG-Chitosan, respectively. *In vitro* bioactivity evaluation in simulated buffer fluid (SBF) solution and antibacterial activity assay predicted that TNT/58S-BG-Chitosan was superior in bone like apatite formation and antibacterial activity against both gram-positive and gram-negative bacteria compared to Ti, TNT and TNT/Chitosan samples, respectively. Results revealed the noticeable MG63 cell attachment and proliferation on TNT/58S-BG-Chitosan coating compared to those of uncoated TNTs. These results confirmed the positive effect of using TNT substrate for natural polymer coating on improved bioactivity of implant.

Key words: Titanium nanotube; Bioactive glass; Chitosan; Antibacterial properties; Bioactivity.

1. Introduction

In the past 30 years, researches on the dental implant materials, techniques and designs have increased and expect to expand in the future due to the rising in the demand for cosmetic dentistry [1, 2]. Statistics provided by the American Association of Oral and Maxillofacial Surgeons show that 69% of adults with ages between 35 to 44 have lost at least one permanent tooth in an accident or because of a failed root canal or tooth decay and gum disease. Furthermore, more than 100,000-300,000 dental implants are implanted each year in the United States because of these reasons [3, 4]. The recent clinical success of these implants has led to an expansion of their use for younger patient populations demanding longer functional lifetime service of these implant devices [2-5]. Therefore, researches have developed in order to develop implants with better properties and extended functional times.

To fabricate dental implants, most of researches have focused on titanium and its alloys [6]. Titanium is one of the inert metals that is extensively used for load-bearing applications due to its excellent biocompatibility, high strength, high toughness, and excellent corrosion resistance and osteointegration [6-8]. Despite these favorable characteristics, the chemically inert surface of titanium implants is not able to form a firm and permanent fixation with the biological tissue to last the lifetime of patients. Moreover, titanium could not able to function as an anti-microbial agent to prevent the peri-implant infections [9, 10]. In addition, titanium alloy implants produce corrosion particles and failed by mechanisms generally related to surface interaction on bone, leading to inflammation with fibrous aseptic loosening or infection and finally implant failure [11]. In order to reach long-term controlling tissue response, developing new and improved medical devices in a more systematic way and at a much faster rate than for native surface, is necessary.

To meet demands of longer functional lifetime service and stability of devices, implant designers and engineers have focused to improve the osseointegration of implants via various surface treatment approaches consisting of plasma-spraying [12-14], grit-blasting [12], acid-etching [12] and anodization techniques [12, 14] as well as osteoconductive coatings [12, 15]. Specific surface properties are often required in order to optimize the function of the device. Although improving or accelerating the osseointegration process is usually the main goal of these surface modification processes, the improvement of biocompatibility and the prevention of bacterial adhesion are also of considerable importance [14, 15]. One of the promising strategies to improve osseointegration is to create surface nano-topography via the anodizing method to reach titania nanotube (TNT) arrays generated over a Ti surface [16]. In recent years, Ti-based implants with nanoscale topographies, especially TNTs have received increasing attention in the area of biomedical applications [16-18]. The electrochemical formation of highly ordered TNT arrays offers a unique surface for biomedical implants. TNT arrays provide available sites for osseointegration and eventually better bone formation, offering both biocompatibility as well as enhanced apatite formation and cell activity [17, 19]. Although there are some results showing TNT possesses improved antibacterial potential [20, 21], there are more evidences about TNT's ability on the reduced antibacterial activity [22, 23]. This conflict it still has not ended. Compared to the currently unmodified Ti surface, TNT supports higher osteoblast adhesion, proliferation and viability which could be helpful for bone formation [19, 24, 25].

Despite the significant characteristics of TNT modified titanium, there are conflicting reports on the TNT effects in vivo during chronic infection, due to differences in surface topographical characteristics and chemical compositions [26-28]. For example, stability of TNTs on Ti implants is crucial, and any delamination or disintegration of TiO_2 nanotube fragments can

initiate toxic responses[29]. To overcome these issues, the second surface coatings consisting of various polymers could be useful. Various types of polymer coatings (i.e. chitosan, poly(lactic glycolic)acid (PLGA)) [30-32] on TNT have been developed. In this regards, chitosan has been offered as a biodegradable natural biopolymer which has been used in many biomedical applications including wound healing [33], drug delivery [33], coating for dental plaque [33, 34], and skin grafting [33] due to the unique properties of chitosan, such as polycationic nature, biocompatibility, biodegradability, bioactivity, antibacterial and antimicrobial efficiency, cheapness and accessibility [33-36]. For instance, Gulati et al. [37] applied chitosan coating on titania nanotube arrays and showed improved osteoblast adhesion on titanium implant [37]. Although chitosan has many positive points as a coating, in order to improve mechanical properties, bioactivity and controlled degradation time, chitosan-ceramic nanocomposites have been proposed [38]. Recently, bioactive glass (BG) has been introduced to stimulate more bone regeneration than other bioactive ceramics [39-41]. Between them, 58S-BG (59% SiO_2, 36% CaO, and 5% P_2O_5) has been widely applied for bone tissue engineering application due to its excellent biocompatibility, bioactivity [39, 42-44]. Moreover, Mortazavi et al. showed that 58S has good antibacterial activity in comparison to other bioactive glass [45]. In this regards, 58S-BG-Chitosan composites has been developed as appropriate scaffolds because of their ability to produce strong bonding between the implant and the surrounding bone [39, 40]. In addition to bioactivity, results demonstrated that nano-sized BG particles specifically 58S-BG have been reported to show antimicrobial activity against various species [39, 46].

Inspired by these elegant approaches, the aim of this research was to develop two-layer nanocomposite coating of TNT/58S-BG-Chitosan and study its biological characteristics consisting of bioactivity, biocompatibility and antibacterial properties. After preparation of TNT

on the surface via anodizing process, nanocomposite coating of 58S-BG-chitosan was developed using dip coating process. Moreover, due to water solubility of chitosan, before 58S-BG-Chitosan coating, alginate was coated on the surface to electro-statistically interact with chitosan. Our goal was to design hybrid coating on Ti based implants to induce rapid healing and have good tissue integration.

2. Materials and methods

2.1. Materials

Ti foil (Sigma-Aldrich, purity=96%) with a thickness of 0.3 mm was used as substrates. Nitric acid (HNO_3 65%), hydrofluoric acid (HF 39%), hydrochloric acid (HCl 37%), acetic acid ($C_2H_4O_2$), acetone $(CH_3)_2CO$, ethanol (C_2H_6O) and glycerol ($C_3H_8O_3$) were purchased from Merck (Germany). Tetraethyl orthosilicate (TEOS: $C_8H_{20}O_4Si$), triethyl phosphate (TEP: $C_6H_{15}O_4P$), calcium nitrate, tetra hydrate ($Ca(NO_3)_2{\cdot}4H_2O$), calcium oxide (CaO), silicon dioxide (SiO_2), phosphorus pentoxide (P_2O_5) and sodium fluoride (NaF) were obtained from Merck (Germany). Chitosan (Mw= 1.4 - 2.2 × 10^5, degree of deacetylation = 85%) and Alginic acid sodium salt (SA) from brown algae (medium viscosity) were provided from Sigma-Aldrich (United States). Deionized distilled (DI) water was used in all the experiments.

2.2. Fabrication of anodized titanium nanotubes

Before anodizing, titanium sheets (10 mm × 30 mm × 0.3 mm) were initially sanded by girt-sized SiC papers (320, 600, 800, 1200 and 2400). Subsequently, the samples were polished with alumina powder. After washing with soap and water, the samples were etched in acid solution (HNO_3: HF: H_2O = 1:1:3) for 15 sec. After subsequent ultrasonication of samples in acetone and ethanol, anodizing process was performed in a 200 ml glycerol solution containing 0.5 wt. %

sodium fluoride (NaF) and 12.5 (v/v)% DI water. Fig. 1 shows the schematic diagram describing the fabrication of two-layer coating processes. In anodizing process, titanium sheet was applied as anode, while platinum foil (40 mm × 80 mm) was used as cathode. The anode and cathode were 3 cm apart and connected to the positive and negative poles of a direct current (DC) power supply (**HANI**electronics, HEP35Extra, 30V-5A), respectively. Voltage and time of anodizing process was optimized to 30 v and 1 h, respectively. During the anodizing process, the solution was magnetically stirred to provide homogenous solution. After anodization, the Ti sheets were washed in DI water and dried at room temperature. Finally, the samples were placed in a furnace at 450 ° C for 1 h for annealing. As prepared titania nanotubes samples were named as TNT.

2.3. Preparation of 58S-BG-Chitosan nanocomposite coating on TiO_2 nanotubes

Before nanocomposite coating, 58S-BG was synthesized using sol-gel process [47]. According to the ternary phase diagram of CaO-SiO_2-P_2O, the composition of 58S-BG was considered 59% SiO_2, 36% CaO, and 5% P_2O_5 in molar percentage. Briefly, 17.5 ml of 2 M hydrochloric acid solution in DI water was prepared and then, 50 ml ethanol, 20.5 ml TEOS and 2 ml TEP were subsequently added to above solution. Consequently, 15 wt.% calcium nitrate ($Ca(NO_3)_2.4H_2O$) was added to the solution and allowed to mix until the solution became clear. After 1 hr mixing, the solution was aged at 60 °C in oven (Nuve dry air FN 120) for 54 h. Finally, following the drying at 130°C for 72 hr, the dried gel was calcined at 1100°C for 1h. In order to prevent the agglomeration of nanoparticles, 58S-BG powder was milled in a planetary ball mill (PM 100) for one 1 h at 250 rpm.

In the next step, chitosan solution with concentration of 1 wt.% in 2 % (v/v) acetic acid solution was prepared at 50 °C. Then, 0.33 wt.% 58S-BG nanoparticles were added to the solution and magnetically stirred for 24 h and then ultrasonicated for 10 min to provide

homogenous distribution of 58S-BG nanoparticles. Before chitosan coating process, the TNT sheets were immersed in 1.25 wt.% alginate solution in 15 % (v/v) glycerol solution at 50 °C for 1 min and dried at room temperature for 1 min, to further increase the electrostatic interaction of chitosan coating. Consequently, the samples were dipped in 58S-BG-Chitosan suspension, in a similar manner. This process was repeated three times to obtain the desired thickness of coating. The samples were named as TNT/58S-BG-Chitosan. In order to study the effect of each component on the properties of the coatings, chitosan was similarly coated on the titania nanotube layer and named as TNT/Chitosan. Moreover, polished Ti substrate was similarly loaded with 58S-BG-Chitosan named as Ti/58S-BG-Chitosan.

2.4. Characterization of the nanocomposite coatings

The surface morphology and chemical composition of the 58S-BG nanopowder as well as coatings was evaluated using scanning electron microscopy (SEM, Philips, XL30) and energy dispersive X-Ray microanalysis (EDS) and element mapping. Before imaging, the samples were sputter coated with a thin layer of gold. Moreover, 250 lengths and 250 diameters were measured for each TiO_2 nanotubes assortment using the ImageJ 1.40 g software. The chemical composition of the prepared 58S-BG-Chitosan coating was verified by attenuated total reflectance-Fourier transform infrared spectroscopy (ATR-FTIR, Bruker tensor), in the range of 500-3700 cm^{-1}. Furthermore, X-ray diffraction (XRD, X'Pert Pro X-ray diffractometer, Phillips, Netherlands) technique was carried out with CuKα radiation (λ=0.154 nm) at a generator voltage of 40 kV. In the present work, Rietveld refinement method was chosen to fit exactly the entire XRD patterns for calculating amount of detected phases. The surface roughness of dried samples was determined using a mechanical contact type stylus-based surface roughness tester, Mitutoyo Surftest SJ-210. Gaussian digital filter with a cut-off length of 2.5 mm and length of 5 mm was

used. Ra, Rq and Rmax were measured a long three different lines on the surface and the average value was considered for further analysis. The surface wettability was determined using sessile drop method by measuring the static water contact angles on a drop-shape system. Briefly, 2 µl of DI water was pipetted on the surface of each sample. Subsequently, the images of the droplets were taken (n=3) and the water contact angle was measured using ImageJ software. The measurements were performed at three different points of the surface and the average of the values were reported.

2.5. In vitro bioactivity and degradation evaluation

In vitro bioactivity of the various coatings was investigated by soaking the samples (n=3) in simulated body fluid (SBF) (pH 7.40) prepared based on Kokubo and Takadama protocol [48]. The samples with size of 5 ×5 mm^2 were soaked in 5 ml SBF solution at 37 ± 0.5°C for 28 days. During this period, the changes in pH of SBF solutions were measured at pre-determined time intervals (0–28 days) using an electrolyte-type pH meter. Moreover, the apatite formation on the surface of the samples as a result of the dissolution and precipitation process of calcium phosphate was investigated by SEM images, as described, previously.

In vitro degradation of coatings was investigated in Dulbecco's Modified Eagle Medium (DMEM-low, Bioidea, Iran) at 37 °C. After 7 days of incubation, the samples were washed with PBS, dried and surface morphology and thickness of coatings were evaluated by SEM imaging.

2.6. Antibacterial activity assay

The antimicrobial activity of samples against two bacteria of *Staphylococcus aureus* and *Escherichia coli* was estimated. The samples with dimension of 2×2 cm^2 were sterilized according to the ASTM E2149. Consequently, each sample was placed in a sterile Petri dish, and

100 µL of (K-12) or *Staphylococcus aureus* (ATCC 12600) grown in 10 mL nutrient broth (approximate formula per liter: beef extract=3.0 g, peptone=5.0 g and distilled water=1000mL, final pH= 6.8± 0.2) at 10^4 -10^5 CFU/mL were added onto their surfaces. Samples were then incubated at 37 ^oC for 1 h, placed into 10 mL of sterile water, and were shaken vigorously for 5 min. Each solution was serially diluted and placed onto agar plates and was incubated at 37 °C for 24 h. The numbers of the colonies formed were counted by quantitation of the colony-forming units (CFU).

2.7. Cell culture

Biocompatibility of coatings was investigated using MG63 cell line (CRL-1427, 14 years, Caucasian, Passage 4) from Royan Institute of Iran. The MG63 cells were cultured in DMEM-low, containing 10 % (v/v) fetal bovine serum (FBS, Bioidea, Iran) and 1 %(v/v) streptomycin/penicillin (Bioidea, Iran) in incubator at 37 ˚C in an atmosphere containing 5% CO_2. The culture medium was changed every 3 days. Before cell seeding, the specimens were washed with phosphate buffer saline (PBS, Bioidea, Iran), sterilized for 60 min in 70% (v/v) ethanol and 6 h under UV light. Consequently, the specimens were immersed in the culture medium consisting for a day before cell seeding. After reaching 70% confluency, the cells were detached with trypsin solution and counted by trypan blue assay. Finally, MG63 cells were seeded on the samples and tissue culture plate (TCP) (control) with a density of 30,000 cells/well. Cells were incubated at 37 °C under 5% CO_2 condition for 7 days and medium was changed every 3 days.

2.7.1. Cell viability study

The relative viability of cells was studied by MTT purchased from Sigma-Aldrich. After 1, 3 and 7 days, the culture medium was removed and MTT solution (0.5 gr/ml) was added to the

cell cultured samples and control. After 4 hr incubation at 37 ˚C under 5% CO_2, the dark blue formazan crystals were dissolved in DMSO (Merck) and kept for 30 min at 37 ˚C. Subsequently, 100 µL of dissolved formazan solution of each sample was moved to 96-well plate and the optical density (OD) of each well was measured with a microplate reader (Biotech) against DMSO (blank) at a wavelength of 490 nm. The relative cell survival (% control) was calculated based on the following equation (2)[49]:

Relative cell survival (% control): $\frac{X_{Sample}-X_b}{X_c-X_b}$ *(2)*

Where X_{Sample}, X_b and X_c were absorbance of the sample, blank (DMSO) and control (TCP), respectively.

2.7.2. Cell morphology study

The morphology of cells seeded on the specimens was investigated by SEM images. After 7 days of culture, the cells were fixed with 2.5% glutaraldehyde (Sigma) for 3 h, rinsed two times with PBS, and dehydrated in the graded concentrations of ethanol (30, 70, 90, 96 and 100 % (v/v)) for 10 min, respectively. Finally, the samples were dried in air and evaluated using SEM imaging.

2.8. Statistical analysis

The data in this study were analyzed using one-way ANOVA analyses and the least significant difference test and reported as mean ± standard deviation (SD). To determine a statistical significance between groups, Tukey-Kramer post-hoc test using GraphPad Prism Software (V.6) was applied and P-value <0.05 was defined as statistically significant. The

overall effect of different coatings on cell viability measured at different time intervals of 1, 3, and 7 days were compared.

3. Results and discussion

3.1. Characterization of two-layer coating

In order to improve the biological properties of Ti based substrates for dental application, two-step coating process including anodizing, followed by 58S-BG-Chitosan coating was applied. Figs. 2A and B show the SEM images of TNTs after anodizing process at two different magnifications. It is clear that the entire surface of titanium substrate is completely covered with uniform TiO_2 nanotubes in vertical alignment. The average inner diameter and wall's thickness of TiO_2 nanotubes were 82 ± 19 nm and 23 ± 9 nm, respectively. Regonini et al. [50] similarly reported the formation of TNTs with diameter of 63±5 nm and thickness of 19±2 nm when NaF containing glycerol/water was used as electrolyte. In another research, TNTs with average diameter of approximately 40 nm were formed using a fluoride containing glycerol electrolyte solution [51]. Previous studies have confirmed that TNTs with diameter of 70–100 nm are acceptable for excellent biocompatibility leading to the formation of elongated cellular morphology and improved cell proliferation [25, 52]; Our results were completely in this safe range suggesting its suitable biocompatibility.

Formation of TNTs was also studied by using current density-time transient curve (Fig. 3A). This curve consisted of three critical stages, as similarly reported in previous paper, confirming the formation of TNTs [53-56]. At stage I, the anodizing process started and the current rapidly reduced to the minimum value due to the formation of a high resistance oxide. In the stage II, the current subsequently raised to maximum as pore nucleation proceed. It might be related to the

decrease in the resistance of the anodic film as more paths were available for ionic species in the electrolyte. In the last stage (stage III), the current reached to a constant value which confirms the formation of TNTs. In this stage, the rate of oxide formation was equal to that of dissolution.

XRD pattern of annealed titania nanotube grown on titanium (at 450˚C for 1 h) is presented in Fig. 3B. In titanium implants, the surface of TiO_2 films are mostly made up of two crystalline polymorphs of titania; rutile, and anatase [56]. Rutile, with the lowest free energy is the stable form of titania while, anatase is metastable polymorph and easily converts into the rutile at high temperatures [56]. After post-growth annealing treatments, it was obvious that amorphous tubes have completely converted into the crystalline anatase or rutile phase. Annealed TNT exhibited an anatase crystalline peak at $2\theta = 25.3^{\circ}$, which is the sharpest peak of crystalline anatase (JCPDS No. 00-004-0477) [57]. Moreover, there were some other peaks at $2\theta = 48.0^{\circ}$ and 82.2° belonging to the crystalline anatase. According to the ICDD (The International Centre for Diffraction Data) and other researches [58-60], Rutile-structured of titania (JCPDS No. 00-004-0551) has series of peaks including a main peak at $2\theta = 27.6^{\circ}$. XRD pattern of produced sample contains no obvious peak at $2\theta = 27.6^{\circ}$, suggesting existence of slight crystalline rutile phase in the TNT, whereas there is stronger evidence about presence of crystalline anatase phase. Also, there are series of distinguishing peaks at $2\theta = 35.2^{\circ}$, 38.4°, 40.2° and 70.6° which are related to Titanium (JCPDS No. 00-044-1294) that reveals, sample contains trace of titanium beneath the titania nanotube.

Rietveld analysis of the XRD result showed that TNT consist of 55± 0.5 % Ti, 41 ± 0.5 % anatase phase and, 4 ± 0.5% rutile phase and confirm the presence of anatase phase in the titania nanotube. In order to reach the highest percentage of anatase phase which is the best condition, crystallization process of amorphous titania should be completed, while the rutile content is

minimal. These two polymorphs have revealed different biological properties. For instance, Kunze et al. [61] reported that anatase structure could provide a suitable environment for the growth of stable bone-like apatite layers upon SBF exposure. Results revealed that anatase could provide stronger integration between tissue and implant, compared to rutile, and can absorb more OH^- and PO_4^{3-} than that of rutile in body fluid, which favors the depositing of bone-like apatite [52, 62]. Moreover, it was found that heat treatment and formation of anatase could significantly enhance the antibacterial property of Ti implants against *S. aureus* and *S. epidermidis* bacteria [21]. Therefore, anatase structure could be desire for biomedical implants.

After TNT preparation via anodizing process, nanocomposite was deposited on the surface of TNTs (TNT/58S-BG-Chitosan) through dip coating process. Before nanocomposite coating, 58S-BG was synthesized using sol-gel method. XRD pattern of 58S-BG (Fig. 4A) showed the presence of crystallite phases consisting of wollastonite ($CaSiO_3$), calcium phosphate ($Ca_4P_2O_9$), and calcium silicate (Ca_2SiO_4). This shows that after heat-treatment at 1100°C, crystallization occurred and the amorphous structure has transformed into the crystalline structure with sharp peaks, similar to the previous research [63]. The main crystalline phase in this powder was wollastonite which revealed the strong interaction with osseous tissue [64].

In order to stabilize 58S-BG-chitosan coating on the surface of the TNT, a layer of sodium alginate was applied on the surface before chitosan dip coating process. SEM image (Fig. 4B) indicated that nanocomposite coating (TNT/58S-BG-Chitosan) completely covered the surface of TNTs. Moreover, 58S-BG nanoparticles were distributed within the surface in cluster-like morphology with size of about 0.76 ± 0.34 mm^2 (Fig. 4B). Moreover, high magnification image (Inset in Fig. 4B) revealed that the size of single particles varied in the range of micrometric (392.953 ± 320.565 μm^2) to nanometric range (743 ± 484 nm^2). EDS mapping analysis (Fig. 4C)

also clearly demonstrated the uniform distribution of bioactive glass nanoparticles within the polymer matrix. Moreover, according to cross section image of nanocomposite coating (Supplementary Fig. S1), the thickness of coating was relatively uniform and was estimated about 55±8 μm.

ATR-FTIR spectrum of TNT/58S-BG-Chitosan are presented in Fig. 5A. In order to confirm the presence of alginate in the coating, nanocomposite coating without sodium alginate (SA-Less) was similarly prepared. Both spectra (with sodium alginate (SA-blend) and without alginate(SA-Less)) consisted of a broad and weak peak at 670 cm^{-1} related to the Ti–O–Ti stretching vibration [65]. Moreover, the specific bonds of 58S-BG at 1076 cm^{-1} (Si-O-Si stretching) and 660 cm^{-1} (ν P-O) could be detected in both FTIR spectra [63, 66, 67]. In the FTIR spectrum of SA-blend made from alginate/58S-BG-Chitosan, a broad peak at 3298 cm^{-1} indicated the presence of extra group and also intermolecular hydrogen bonding between alginate with chitosan and 58S-BG. It was interesting to see that amide I (ν C=O), amide II (ν N-H) and amide III (ν C-N) peaks of chitosan moved toward higher frequency, in their expected peak area at 1650 cm^{-1}, 1550 cm^{-1} and 1328 cm^{-1}, respectively, while the presence of a peak shoulder at 1590 cm^{-1} suggested a new intermolecular interaction in the blend. In addition, the intense increase in the peak at 1415 cm^{-1} confirmed that the carboxylate group of SA has been dissociated to COO^- group which can make ionic interaction with cationic groups in the bioactive glass or NH_3^+ groups of the chitosan [68]. The fact that chitosan amide I and amide II peak did not show any shift exclude the probability of high ionic interaction between sodium alginate and chitosan. It worth mentioning that in experimental procedures, blending the sodium alginate and chitosan did not change the viscosity of the blend but when chitosan-58S-BG was mixed with sodium alginate, a highly viscose hydrogel was formed. That was the reason a layer of alginate

was coated on titanium first and the chitosan-58S-BG layer was applied and the resulting layer had good stability and did not dissolve in the water easily. In addition, the formation of a peak at 1590 cm^{-1} could possibly confirm the ionic interaction between 58S-BG and chitosan.

Hydrophilicity is one of the most important properties of coatings affecting the biological properties such as bacteria/cell adhesion and spreading and could be determined by water contact angle test method. The wettability of samples was determined using contact angle measurement (Fig. 5B). Results revealed that the hydrophilicity of samples are directly related to their surface roughness and chemical composition. Wennerberg et al. [69] suggested that three parameters, including the mean roughness (roughness average) (R_a), the root mean square roughness (R_q), and the maximum roughness depth (R_{max}), could be useful to evaluate the surface roughness of the samples (Table 1). After loading 58S-BG-Chitosan on Ti sheets, surface roughness and contact angle were not significantly changed ($P>0.05$) (Table 1). However, after anodizing (TNT sample) the surface roughness of Ti sheets significantly enhanced (3.4 times) from 132 ± 26 nm to 449 ± 15 nm ($P<0.05$). In this condition, water contact angle considerably reduced (2 times). Previous researches similarly reported the enhanced hydrophilicity of anodized Ti and showed that it could be due to the formation of pores and sites for liquid penetration leading to reduced contact angle and improved hydrophilicity of sample [20, 65, 70, 71].

After surface coating of anodized Ti sheets using chitosan (TNT/Chitosan sample), the mean roughness reduced from 449 nm to around 86 nm leading to significantly enhanced contact angle (2.7 times) ($P<0.05$) which showed less hydrophilicity of chitosan coated samples. On the other hand, incorporation of 58S-BG nanopowder into the coating (TNT/58S-BG-Chitosan) enhanced the average surface roughness from 86 ± 3 nm (at TNT/Chitosan) to 143 ± 41 nm, (at TNT/58S-BG-Chitosan) and reduced water contact angle from 91.5± 6.3° (at TNT/Chitosan) to 66.2 ± 2.9°

(at TNT/58S-BG-Chitosan) which indicated the increased hydrophilicity. Our results showed that all samples were relatively hydrophilic. However, development of TNTs and/or secondary coating on the surface of Ti sheets resulted in modulated water contact angle due to the critical role of surface roughness on the hydrophilicity of samples. Similarly, Wenzel et al [72] showed that higher surface roughness resulted in improved wettability of surfaces, due to greater the number of bonding sites between the water droplet and the surface of samples.

3.2. Bioactivity and degradation evaluation of the coatings

The formation of bone like apatite on the surface of implants is required to promote osteoconduction, accelerate bone repair and ensure implant's success. The bone-like apatite formation on the various samples was investigated via in vitro immersion of samples in SBF for 28 days. SEM images of samples after soaking in SBF solution are presented in Fig. 6. While Ti specimen did not induce any apatite formation on its surface, precipitated apatite could be detected on the other samples after immersion in SBF. However, depending on the surface chemistry and roughness, the concentration of deposited bone-like apatite on the samples was different. Our results confirmed that 58S-BG and TNT layer were two important components in bone-like apatite formation ability. Although the chemical composition of spontaneous titania thin layer on titanium and TNT were similar, different surface roughness and subsequent wettability resulted in drastically different responses during immersion in SBF solution. In contrary to titania thin layer on titanium, nanotube-like structures of TNT (Fig. 6C) provided more surface area and more reactive sites for nucleation of apatite cluster. Bayram et al. [65] reported similar results on the bioactivity of TNTs compared to the untreated titanium. Similarly, Li et al. [73] stated the excellent bioactivity of TNT arrays due to their high specific surface area. Moreover, Fig. 6D showed that less apatite formed layer on TNT/Chitosan, that is strange results

for the polymer that consider in many researches as bioactive compound [36]. It might be due to its relatively weak wettability, smooth surface and lack of nucleation sites for the attenuated formation of apatite. SEM image of Ti/58S-BG-Chitosan (Fig. 6B) and TNT/58S-BG-Chitosan (Fig. 6E) showed that the apatite layer has covered the entire surface, revealing that presence of bioactive glass alongside chitosan had significant impact on the bioactivity of coatings. Incorporation of bioactive glass within chitosan matrix stimulatory changed the surface roughness and chemical composition of surface and accelerated the formation of apatite due to nature of bioactive glass. Mota et al. [74] similarly confirmed the improved bioactive potential of bioactive glass incorporated chitosan. In addition, the size of apatite clusters formed on the TNT/58S-BG-Chitosan were much bigger than that of Ti/58S-BG-Chitosan, due to the higher surface roughness and wettability of the former.

The pH value of SBF solution at different time points of immersing in SBF is presented in Fig. 6F. At first day, pH value of SBF solution noticeably increased, depending on the sample type. However, each coating had a specific pH value range changed over time. The rapid release of alkali ions, Ca and P ions, was supposed to cause the similarly rapid increase in pH value inside the solution. This process was effectively happened in soaking of Ti/58S-BG-Chitosan and TNT/58S-BG-Chitosan samples. After the initial rapid increase in pH value, it slowly reduced until the day 28 in all specimens due to the precipitation of calcium phosphates and carbonates from solution on the sample surface [54]. While consumption of Ca and P ions in the SBF solution was the first step of apatite nucleation in bioactive glass based coatings, apatite nucleation on TNT started with the Ti-OH group formation on the TiO_2 layer. When TNT soaked in SBF solution, the surface was slightly negatively charged which attract Ca^{2+}, and consequently PO_4^{-3} and CO_3^{-2} ions from the SBF to form apatite on the surface. This process

resulted in increase in H^+ concentration and, hence, decrease in pH value of solution, according to the following equation [75]:

$HCO_3^- \rightarrow CO3^{-2} + H^+$ and $HPO_4^{-2} \rightarrow PO_4^{-3} + H^+$

As the biologic response of the samples strictly depends on the morphology of coating, it was evaluated using soaking the samples in DMEM for 7 days at 37 °C. SEM images of the surface and cross-section of Ti/58S-BG-Chitosan and TNT/58S-BG-Chitosan coatings after incubating in DMEM at 37 °C are presented in Supplementary Figs. S2A and B. Our results confirmed that the morphology of the coatings during immersing in DMEM did not significantly change. However, the thickness of coatings were nearly changed, depending on the sample. While the thickness of TNT/58S-BG-Chitosan coating was estimated about 21±1.5µm, it was reduced to 11±2.7µm µm at Ti/58S-BG-Chitosan sample. The slower degradation rate of TNT/58S-BG-Chitosan compared to Ti/58S-BG-Chitosan coating might be due to the presence of TNT layer which mechanically interact with 58S-BG-chitosan layer. Moreover, SEM image of top-veiw of these two coatings confirmed that after 7-day incubation in DMEM, Ti/58S-BG-Chitosan still covered whole surface with some short cracks. However, TNT/58S-BG-Chitosan nearly degraded after 7 days of incubation.

3.3. Antibacterial activity assay

Fig. 7 shows the difference in the antibacterial properties of samples (Ti/58S-BG-Chitosan, TNT, TNT/Chitosan, and TNT/58S-BG-Chitosan) against Gram-negative bacterium *E. coli* and gram positive bacterium *S. aureus* in comparison to that of pure Ti surface. Results revealed that antibacterial activity of TNT against both positive and gram negative bacteria decreased compared to that of Ti which was in agreement with other research findings. It was probably

related to the special nanometer sized topographies and consequently higher hydrophilicity of nanotube surface resulted in more bacterial adhesion which in return reduced the antibacterial activity of the surface [22, 23]. On the other hand, chitosan and 58S-BG-chitosan coatings on the surface increased the antibacterial activity of the implant against both bacteria *S. aureus* and *E.coli*. The result was expected as both chitosan and 58S-BG are bioactive polymers with intrinsic antibacterial property. Therefore, combining both chitosan and 58S-BG led to higher antibacterial activity in comparison to the chitosan alone, and the role of 58S-BG was completely match to other findings [45]. It was noticeable that coating of the chitosan and 58S-BG-chitosan layer on the surface of TNT sample clearly increased the antibacterial activity by 69 ± 2% and 89 ± 3% against *E. coli* and by 65 ± 5% and 71 ± 3% against *S. aureus* in comparison to Ti. These results showed that the presence of titania nanotube layer played an important role in improvement of the antibacterial property.

Considering Fig. 8, it was suggested that nanotube layer mechanically interacted with 58S-BG-chitosan leading to the presence of higher amount of antibacterial polymer on the surface (supplementary Fig S2). Higher amount of coated biopolymer in addition to higher roughness synergistically increased the antibacterial activity of the surface. similarly, in other finding, the crucial role of surface roughness on the antibacterial properties was confirmed [76, 77]. This clearly showed the positive impact of TNT on the increase of antibacterial activity of the polymer coated implants which was of great importance. In general, according to the results obtained, the impact of different coatings on Gram-negative bacterium was slightly higher than Gram-positive bacteria.

3.4. Cell Culture

The biocompatibility of surface modified samples was investigated using evolution of MG63

cell attachment and proliferation. SEM images of MG63 cells cultured for 7 days on the various samples are presented in Fig. 9. The red arrows in the figures are pointed to the cells attached and spread on the various coatings after 7 days of culture. While a limited number of cells were attached on the control titanium foil (Ti) (Fig. 8A), cells adhered tightly to the surface of other samples with various morphologies, depending on the sample type. For instance, few cells spread on the surface of the Ti/58S-BG-Chitosan with a flatter morphology and noticeable filopodia and lamellipodia extensions (Fig. 9B), while on TNTs, more MG63 cells accumulated on the surface and covered most of cracks and fissures (Fig. 9C). Similar result was reported by Zhang et al. who showed the formation of this layer on TNTs [78]. In contrary, less cells covered the surface of TNT/Chitosan (Fig. 9D) with little spreading. However, the outcomes indicated that cells on TNT well spread compared to that of Ti, Ti/58S-BG-Chitosan, and TNT/Chitosan samples. In other research, Yang et al. [79] similarly showed poor spreading of Ti and TNT/Chitosan compared to TNT. Moreover, the cells seeded on the TNT/58S-BG-Chitosan (Fig. 9E) preserved a well spread osteoblast-like cells covering most of cracks. Moreover, compared to Ti/58S-BG-Chitosan coating, cells with more filopodia and lamellipodia extensions could be detected on TNT/58S-BG-Chitosan.

Fig. 9F showed the cell retention modulation (fraction of coating surface covered with cells) as a function of sample type. Cell retention was estimated based on the changes in the quintuple coating by studying three specimens for every coating. Increasing in the surface roughness and hydrophilicity by anodizing resulted in dramatically enhanced cell retention ($P < 0.05$) from 0.09 ± 0.02 (on Ti) to 0.38 ± 0.01 (on TNT). On the other hand, TNT/Chitosan with smoother surface and reduced hydrophilicity had slightly lower cell retention (0.35 ± 0.02) compared to the TNT surfaces. Yang et al. [79] reported similar result, but related that to the slight cytotoxicity of the

chitosan. Additionally, the friction of attached cells on the surfaces of the TNT/58S-BG-Chitosan was significantly higher than on other specimens ($P<0.05$). Noticeably, after 7 days of culture of MG63 cells on TNT/58S-BG-Chitosan, the cell area was 1.3-fold greater than on TNT confirming the stimulatory role of bioactive glass and TNT on the cell area enlargement, which again confirmed that might be due to the enhanced surface roughness and hydrophilic nature of coating has great impact on the bioactivity of surfaces.

In order to examine the metabolic activity of MG63 cells seeded on the specimens, MTT assay was performed. Fig. 10 reveals that survival of cells cultured on each sample significantly enhanced with increasing the culture time from day 1 to day 7 ($P < 0.05$). For instance, the metabolic activity of cells cultured on the TNT enhanced from 67.2 ± 7.1 (% control) (at day 1) to 138.6 ± 4.7 (% control) (at day 7) ($P < 0.05$). Moreover, the MTT assay of TNT/58S-BG-Chitosan revealed that the proliferation of MG63 cells enhanced from 74.4 ± 2.2 (% control) (at day 1) to 215.5 ± 14.2 (% control) (at day 7) ($P < 0.05$). However, different trends could be detected between various samples confirming the role of samples on the proliferation of MG63 cells. For instance, the number of metabolically active cells grown on the TNT was 1.6-fold higher than that of on the Ti ($P < 0.05$). There were some similar results that showed better proliferation of cells on TNTs over Ti, which could be due to the effects of surface roughness and hydrophilicity on the proliferation of cells [37, 79].

Likewise, the cell proliferation on TNT/Chitosan was higher than that on Ti (1.63 times) at day 7 ($P<0.05$), while no significant difference was found among TNT and TNT/Chitosan. Recently, chitosan coating on TNTs was similarly investigated and contradictory results were reported by researchers. For instance, Gulati et al. [37] observed better cell proliferation on the chitosan coating related to the positively charged chitosan chains which could promote protein

absorption and subsequently cell adhesion. However, Yang et al. [79] reported different result and showed the slight cytotoxicity of the chitosan. Our result showed no significant difference between TNT and TNT/Chitosan, probably due to the different roughness, hydrophilicity and bioactivity of the surfaces. Coating of chitosan over TNTs resulted in reduced surface roughness and hydrophilicity in comparison to the TNT coated surface leading to decreased cell's attachment and proliferation. In the other hand, according to the previous findings, chitosan considered as good bioactive polymer which resulted in higher cell attachment and proliferation. The overall outcome of these opposite effects was the almost equal cell attachment on both chitosan and TNT coated surfaces.

Our results indicated that the cells on TNT/58S-BG-Chitosan exhibited a significantly higher cell survival than those on Ti/58S-BG-Chitosan (2 times) and TNT/Chitosan (1.5 times) at 7 days ($P<0.05$). The difference between Ti/58S-BG-Chitosan and TNT/58S-BG-Chitosan could be due to the presence of TNTs beneath 58S-BG-chitosan as a coating promoter, which strongly enhanced cell survival. In addition, the increased surface roughness and hydrophilicity of implant due to the incorporation of bioactive glass into the polymer had positive effect in the accelerating cell adhesion and proliferation, thereby promoting cell retention. These results were in accordance with the antibacterial test results, where coating of biopolymers on TNT coated titanium surface led to the higher antibacterial activity. In conclusion, we demonstrated that hybrid TNT/58S-BG-chitosan coating on titanium could highly promote MG63 cell adhesion, spreading, proliferation and antibacterial activity.

4. Conclusion

In the present study, titania nanotube (TNT)/58S-BG-Chitosan coating was developed on titanium substrates by combination of TNTs and degradable 58S-BG-chitosan coating. While

TNT was developed using anodizing process, 58S-BG-Chitosan layer was consequently formed on the surface of TNT layer via dip coating process. While TNT structure with high porosity exhibited hydrophilic and approximately good biological characteristics, it revealed weak antibacterial property. Addition of 58S-BG-chitosan coating on TNTs provided special degradable microporous structure with high roughness, offering desirable space for cell ingrowth and attachment. Notably, the 58S-BG-chitosan coating on the nanotube layer clearly improved the antibacterial properties compared to TNT sample. Moreover, our study demonstrated that TNT/58S-BG-Chitosan coating on titanium represented conspicuously good in vitro osteoconductivity when compared to Ti and TNT samples. In summary, we demonstrated that the TNT/58S-BG-Chitosan coating with good ability for facilitating the attachment, spreading and proliferation of MG63 might have great potential for the improvement of osseointegration and repair of bone defects.

Acknowledgments

We acknowledge Dr. Keyvan Raeissi of the Faculty of Materials Engineering, the Coating Laboratory for the help on anodizing test. This work was supported by Faculty of Materials Engineering in Isfahan University of Technology.

References

[1] A. Alani, M. Kelleher, K. Hemmings, M. Saunders, M. Hunter, S. Barclay, M. Ashley, S. Djemal, K. Bishop, U. Darbar, P. Briggs, J. Fearne, *Balancing the risks and benefits associated with cosmetic dentistry - a joint statement by UK specialist dental societies,* Br. Dent. J. **218**(2015) 543-8

[2] M. C. Dixon, R. R. Brown, D. Parsch, R. D. Scott, *Modular Fixed-Bearing Total Knee Arthroplasty with Retention of the Posterior Cruciate Ligament,* J. Bone. & Join. Surge. **87**(2005) 598–603

[3] F. E. Lambert, H. P. Weber, S. M. Susarla, U. C. Belser, G. O. Gallucci, *Descriptive analysis of implant and prosthodontic survival rates with fixed implant-supported rehabilitations in the edentulous maxilla,* J. Periodontol. **80**(2009) 1220-30

[4] A. Gupta, M. Dhanraj, G. Sivagami, *Status of surface treatment in endosseous implant: a literary overview,* Indian. J. Dent. Res. **21**(2010) 433-8

[5] P. Simonis, T. Dufour, H. Tenenbaum, *Long-term implant survival and success: a 10-16-year follow-up of non-submerged dental implants,* Clin. Oral. Implants. Res. **21**(2010) 772-7

[6] X. Liu, P. Chu, C. Ding, *Surface modification of titanium, titanium alloys, and related materials for biomedical applications,* Mat. Sci. Engin. R. Rep. **47**(2004) 49-121

[7] H. Wang, C. Lin, R. Hu, *Effects of structure and composition of the CaP composite coatings on apatite formation and bioactivity in simulated body fluid,* App. Sur. Sci. **255**(2009) 4074-4081

[8] T. O. Albrektsson, C. B. Johansson, L. Sennerby, *Biological aspects of implant dentistry: osseointegration,* Periodont. 2000,. **4**(2000) 58-73

[9] F. Suska, S. Svensson, A. Johansson, L. Emanuelsson, H. Karlholm, M. Ohrlander, P. Thomsen, *In vivo evaluation of noble metal coatings,* J. Biomed. Mater. Res. B. Appl. Biomater. **92**(2010) 86-94

[10] D. M. Brunette, P. Tengvall, M. Textor, P. Thomsen, *Titanium in Medicine, Material Science, Surface Science, Engineering, Biological Responses and Medical Applications*, Springer, 2001, 1018.

[11] Petersen, R. C., *Titanium Implant Osseointegration Problems with Alternate Solutions Using Epoxy/Carbon-Fiber-Reinforced Composite,* Metals. Basel. **4**(2014) 549-569

[12] L. Le Guehennec, A. Soueidan, P. Layrolle, Y. Amouriq, *Surface treatments of titanium dental implants for rapid osseointegration,* Dent. Mater. **23**(2007) 844-54

[13] D. M. Dohan Ehrenfest, P. G. Coelho, B. S. Kang, Y. T. Sul, T. Albrektsson, *Classification of osseointegrated implant surfaces: materials, chemistry and topography,* Tren. Biotechnol. **28**(2010) 198-206

[14] P. Mandracci, F. Mussano, P. Rivolo, S. Carossa, *Surface Treatments and Functional Coatings for Biocompatibility Improvement and Bacterial Adhesion Reduction in Dental Implantology,* Coat. **6**(2016) 7

[15] B. G. Zhang, D. E. Myers, G. G. Wallace, M. Brandt, P. F. Choong, *Bioactive coatings for orthopaedic implants-recent trends in development of implant coatings,* Int. J. Mol. Sci. **15**(2014) 11878-921

[16] J. K. Lee, D. S. Choi, I. Jang, W. Y. Choi, *Improved osseointegration of dental titanium implants by TiO2 nanotube arrays with recombinant human bone morphogenetic protein-2: a pilot in vivo study,* Int. J. Nanomed. **10**(2015) 1145-54

[17] Q. Wang, J. Y. Huang, H. Q. Li, Z. Chen, A. Z. Zhao, Y. Wang, K. Q. Zhang, H. T. Sun, S. S. Al-Deyab, Y. K. Lai, *TiO2 nanotube platforms for smart drug delivery: a review,* Int. J. Nanomedicine. **11**(2016) 4819-4834

[18] L. Zhao, H. Wang, K. Huo, L. Cui, W. Zhang, H. Ni, Y. Zhang, Z. Wu, P. K. Chu, *Antibacterial nano-structured titania coating incorporated with silver nanoparticles,* Biomateri. **32**(2011) 5706-16

[19] T. Gong, J. Xie, J. Liao, T. Zhang, S. Lin, Y. Lin, *Nanomaterials and bone regeneration,* Bone. Res. **3**(2015) 15029

[20] Z. Peng, J. Ni, K. Zheng, Y. Shen, X. Wang, G. He, S. Jin, T. Tang, *Dual effects and mechanism of TiO2 nanotube arrays in reducing bacterial colonization and enhancing C3H10T1/2 cell adhesion,* Int. J. Nanomedicine. **8**(2013) 3093-105

[21] B. Ercan, E. Taylor, E. Alpaslan, T. J. Webster, *Diameter of titanium nanotubes influences anti-bacterial efficacy,* Nanotech. **22**(2011) 295102

[22] S. D. Puckett, E. Taylor, T. Raimondo, T. J. Webster, *The relationship between the nanostructure of titanium surfaces and bacterial attachment,* Biomate. **31**(2010) 706-713

[23] S. Mei, H. Wang, W. Wang, L. Tong, H. Pan, C. Ruan, Q. Ma, M. Liu, H. Yang, L. Zhang, Y. Cheng, Y. Zhang, L. Zhao, P. K. Chu, *Antibacterial effects and biocompatibility of titanium surfaces with graded silver incorporation in titania nanotubes,* Biomat. **35**(2014) 4255-65

[24] K. C. Popat, L. Leoni, C. T. Grimes, T. A. Desai, *Influence of engineered titania nanotubular surfaces on bone cells,* Biomateri. **28**(2007) 3188-97

[25] E. Gongadze, D. Kabaso, S. Bauer, T. Slivnik, P. Schmuki, U. van Rienen, A. Iglic, *Adhesion of osteoblasts to a nanorough titanium implant surface,* Int. J. Nanomedicine. **6**(2011) 1801-16

[26] A. Wennerberg , T. Albrektsson *On implant surfaces: a review of current knowledge and opinions,* Int. J Oral. Maxillofac. Implants. **25**(2010) 63–74

[27] L. M. Bjursten, L. Rasmusson, S. Oh, G. C. Smith, K. S. Brammer, S. Jin, *Titanium dioxide nanotubes enhance bone bonding in vivo,* J. Biomed. Mater. Res. A. **92**(2010) 1218-24

[28] C. M. Sayes, R. Wahi, P. A. Kurian, Y. Liu, J. L. West, K. D. Ausman, D. B. Warheit, V. L. Colvin, *Correlating nanoscale titania structure with toxicity: a cytotoxicity and inflammatory response study with human dermal fibroblasts and human lung epithelial cells,* Toxicol. Sci. **92**(2006) 174-85

[29] D. Losic, A. Santos, *Electrochemically Engineered Nanoporous Materials Methods Properties and Applications*, Springer, 2015.

[30] T. Wang, Z. Weng, X. Liu, K. W. K. Yeung, H. Pan, S. Wu, *Controlled release and biocompatibility of polymer/titania nanotube array system on titanium implants,* Bioact. Mat. **2**(2017) 44-50

[31] M. S. Aw, M. Kurian, D. Losic, *Non-eroding drug-releasing implants with ordered nanoporous and nanotubular structures: concepts for controlling drug release,* Biomater. Sci. **2**(2014) 10-34

[32] M. S. Aw, K. Gulati, S. Ramakrishnan, J. Addai-Mensah, D. Losic, *The electrochemicaly engineered nanotubular surfaces for controlled and sustained delivery of drugs and drug carriers*. 2011.

[33] F. Ezoddini-Ardakani, A. Navab Azam, S. Yassaei, F. Fatehi, G. Rouhi, *Effects of chitosan on dental bone repair,* Health. **03**(2011) 200-205

[34] U. T. Kalyoncuoglu, B. Yilmaz, S. Gungor, *Evaluation of the chitosan-coating effectiveness on a dental titanium alloy in terms of microbial and fibroblastic attachment and the effect of aging,* Materiali. tehnologije. **49**(2015) 925-931

[35] N. Poth, V. Seiffart, G. Gross, H. Menzel, W. Dempwolf, *Biodegradable chitosan nanoparticle coatings on titanium for the delivery of BMP-2,* Biomolec. **5**(2015) 3-19

[36] Prabaharan, M., *Bioactivity of Chitosan Derivative,* (2014) 1-14

[37] K. Gulati, S. Ramakrishnan, M. S. Aw, G. J. Atkins, D. M. Findlay, D. Losic, *Biocompatible polymer coating of titania nanotube arrays for improved drug elution and osteoblast adhesion,* Acta. Biomater. **8**(2012) 449-56

[38] C. Paluszkiewicz, E. Stodolak, M. Hasik, M. Blazewicz, *FT-IR study of montmorillonite-chitosan nanocomposite materials,* Spectrochim. Acta. A. Mol. Biomol. Spectrosc. **79**(2011) 784-8

[39] K. Maji, S. Dasgupta, K. Pramanik, A. Bissoyi, *Preparation and Evaluation of Gelatin-Chitosan-Nanobioglass 3D Porous Scaffold for Bone Tissue Engineering,* Int. J. Biomater. **2016**(2016) 9825659

[40] K. R. Mohamed, H. H. Beherei, Z. M. El-Rashidy, *In vitro study of nano-hydroxyapatite/chitosan-gelatin composites for bio-applications,* J. Adv. Res. **5**(2014) 201-8

[41] Hench, L. L., *Opening paper 2015- Some comments on Bioglass: Four Eras of Discovery and Development,* Biomed. glass. **1**(2015)

[42] H. Li, R. Du, J. Chang, *Fabrication, characterization, and in vitro degradation of composite scaffolds based on PHBV and bioactive glass,* J. Biomater. Appl. **20**(2005) 137-55

[43] W. Y. Gong, Y. M. Dong, X. F. Chen, B. Karabucak, *Nano-sized 58S Bioactive Glass Enhances Proliferation and Osteogenic Genes Expression of Osteoblast-like Cells,* Chine. J. Dent. Res. **15**(2012) 145-152

[44] R. C. Bielby, R. S. Pryce, L. L. Hench , J. M. Polak, *Enhanced Derivation of Osteogenic Cells from Murine Embryonic Stem Cells after Treatment with Ionic Dissolution Products of 58S Bioactive Sol–Gel Glass,* Tissue. Eng. **11**(2005) 479-88

[45] V. Mortazavi, M. M. Nahrkhalaji, M. H. Fathi, S. B.Mousavi, B. N.Esfahani, *Antibacterial effects of sol-gel-derived bioactive glass nanoparticle on aerobic bacteria,* J. Biomed. Mater. Res. A. **94**(2010) 160-8

[46] M. Erol-Taygun, K. Zheng, A. R. Boccaccini, *Nanoscale Bioactive Glasses in Medical Applications,* Inter. J. App. Gla. Sci. **4**(2013) 136-148

[47] R. Li, A. Clark, L. Hench, *An Investigation of Bioactive Glass Powders by Sol-Gel Processing,* J. App. Biomate. **2**(1991) 231-239

[48] T. Kokubo, H. Takadama, *How useful is SBF in predicting in vivo bone bioactivity?,* Biomater. Sci. **27**(2006) 2907-15

[49] N. Golafshan, M. Kharaziha, M. H. Fathi, *Tough and conductive hybrid graphene-PVA: Alginate fibrous scaffolds for engineering neural construct,* Carbon. **111**(2017) 752-763

[50] D. Regonini, A. Satka, D. W. E. Allsopp, A. Jaroenworaluck, R. Stevens, C. R. Bowen, *Anodised Titania Nanotubes Prepared in a Glycerol/NaF Electrolyte,* J. Nanoscien. Nanotech. **9**(2009) 4410-4416

[51] J. M. Macak, H. Tsuchiya, L. Taveira, S. Aldabergerova, P. Schmuki, *Smooth anodic TiO2 nanotubes,* Angew. Chem. Int. Ed. Engl. **44**(2005) 7463-5

[52] Y. Wang, C. Wen, P. Hodgson, L. Yuncang, *Biocompatibility of TiO2 nanotubes with different topographies,* J. Biomed. Mater. Res. A. **102**(2014) 743–751

[53] A. Valota, D. J. LeClere, P. Skeldon, M. Curioni, T. Hashimoto, S. Berger, J. Kunze, P. Schmuki, G. E. Thompson, *Influence of water content on nanotubular anodic titania formed in fluoride/glycerol electrolytes,* Electrochimica. Acta. **54**(2009) 4321-4327

[54] C. Cao, J. Li, X. Wang, X. Song, Z. Sun, *Current characterization and growth mechanism of anodic titania nanotube arrays,* J. Mat. Resea. **26**(2011) 437-442

[55] A. Valota, M. Curioni, D. J. Leclere, P. Skeldon, P. Falaras, G. E. Thompson, *Influence of Applied Potential on Titanium Oxide Nanotube Growth,* J. Electrochemic. Soc. **157** (2010) 243-247

[56] D. Regonini, C. R. Bowen, A. Jaroenworaluck, R. Stevens, *A review of growth mechanism, structure and crystallinity of anodized TiO2 nanotubes,* Mat. Sci. Engin. **74**(2013) 377-406

[57] K. Shankar, G. K. Mor, H. E. Prakasam, S. Yoriya, M. Paulose, O. K. Varghese, C. A. Grimes, *Highly-ordered TiO2 nanotube arrays up to 220 µm in length: use in water photoelectrolysis and dye-sensitized solar cells,* Nanotechn. **18**(2007) 065707

[58] A. Mazare, G. Totea, C. Burnei, P. Schmuki, I. Demetrescu, D. Ionita, *Corrosion, antibacterial activity and haemocompatibility of TiO2 nanotubes as a function of their annealing temperature,* Cor. Sci. **103**(2016) 215-222

[59] C. Cao, G. Zhang, X. Song, Z. Sun, *Morphology and Microstructure of As-Synthesized Anodic TiO2 Nanotube Arrays,* Nanoscal. Resea. Lett. **6**(2011)

[60] J. M. Macak, H. Hildebrand, U. Marten-Jahns, P. Schmuki, *Mechanistic aspects and growth of large diameter self-organized TiO2 nanotubes,* J. Electroanalyti. Chem. **621**(2008) 254-266

[61] J. Kunze, L. Müller, J. Macak, P. M. Greil, P. Schmuki, F. A. Müller, *Time-dependent growth of biomimetic apatite on anodic TiO2 nanotubes,* Electrochimca. Acta. **53**(2008) 6995-7003

[62] F. Ahu Akin, H. Zreiqat, S. Jordan, L. Hanley, *Preparation and analysis of macroporous TiO2 films on Ti surfaces for bone–tissue implants,* J. Biomed. Mat. Res. **57**(2001) 588–596

[63] M. T. Dehaghani, M. Ahmadian, M. H. Fathi, *Synthesis, Characterization, and Bioactivity Evaluation of Amorphous and Crystallized 58S Bioglass Nanopowders,* Inter. J. App. Cera. Tech. **12**(2015) 867-874

[64] J. R. Jones, L. M. Ehrenfried, L. L. Hench, *Optimising bioactive glass scaffolds for bone tissue engineering,* Biomate. **27**(2006) 964-73

[65] C. Bayram, M. Demirbilek, N. Çalı¸skan, M. E. Demirbilek, E. B. Denkba¸s, *Osteoblast Activity on Anodized Titania Nanotubes: Effect of Simulated Body Fluid Soaking Time,* J. Biomed. Nanotech. **8**(2011) 1–9

[66] P. Saravanapavan, J. R. Jones, R. S. Pryce, L. L. Hench, *Bioactivity of gel–glass powders in the CaO-SiO2 system: A comparison with ternary (CaO-P2O5-SiO2) and quaternary glasses (SiO2-CaO-P2O5-Na2O),* J. Biomed. Mat. Res. Part. A. **66A**(2003) 110–119

[67] G. Theodorou, O. M. Goudouri, E. Kontonasaki, X. Chatzistavrou, L. Papadopoulou, N. Kantiranis, K. M. Paraskevopoulos, *Comparative Bioactivity Study of 45S5 and 58S Bioglasses in Organic and Inorganic Environment,* Biocera. Deve. App. **1**(2011) 1-4

[68] Yuvarani, I, et al., *Preparation and characterization of curcumin coated chitosan-alginate blend for wound dressing application,* Journal of Biomaterials and Tissue Engineering. **2**(2012) 54-60

[69] A. Wennerberg , T. Albrektsson, *Suggested guidelines for the topographic evaluation of implant surfaces,* J. Oral. Maxi. Imp. **15**(2000) 331-344

[70] G. Liu, K. Du, K. Wang, *Surface wettability of TiO2 nanotube arrays prepared by electrochemical anodization,* App. Sur. Sci. **388**(2016) 313-320

[71] A. Rajyalakshmi, B. Ercan, K. Balasubramanian, T. J.Webster, *Reduced adhesion of macrophages on anodized titanium with select nanotube surface features,* Int. J. Nanomed. **6**(2011) 1765-71

[72] Wenzel, R. N., *Resistance of solid surfaces to wetting by water,* Indus. engin. chem. **28**(1936) 988

[73] M. Li, L. Xiao, R. Xiufeng, *Synthesis and bioactivity of highly ordered TiO2 nanotube arrays,* App. Surf. Sci. **255**(2008) 365-367

[74] J. Mota, N. Yu, S. G. Caridade, G. M. Luz, M. E. Gomes, R. L. Reis, J. A. Jansen, X. F. Walboomers, J. F. Mano, *Chitosan/bioactive glass nanoparticle composite membranes for periodontal regeneration,* Acta. Biomater. **8**(2012) 4173-80

[75] S. Jebahi, H. Oudadesse, E. Wers, J. Elleuch, H. Elfekih, H. Keskes, X. V. Bui, A. Elfeki, *Effect of pH and Ionic Exchange on the Reactivity of Bioglass/Chitosan Composites Used as a Bone Graft Substitute,* Inter.l J. Chem.l, Mol., Nu., Mat. and Metal. Engi. **7**(2013)

[76] Yoda, Itaru, et al., *Effect of surface roughness of biomaterials on Staphylococcus epidermidis adhesion,* BMC Microbiology. **14**(2014)

[77] Lewandowska, Zaneta, et al., *The evaluation of the impact of titania nanotube covers morphology and crystal phase on their biological properties,* Journal of Materials Science: Materials in Medicine. **26**(2015)

[78] H. Zhang, S. Yang, N. Masako, D. J. Lee, L. F. Cooper, C. C. Ko, *Proliferation of preosteoblasts on TiO2 nanotubes is FAK/RhoA related,* RSC. Adv. **5**(2015) 38117-38124

[79] Y. Yang, H. Ao, Y. Wang, W. Lin, S. Yang, S. Zhang, Z. Yu, T. Tang, *Cytocompatibility with osteogenic cells and enhanced in vivo anti-infection potential of quaternized chitosan-loaded titania nanotubes,* Bone. Res. **4**(2016) 16027

Figure caption:

Figure 1. Schematic diagram describing the fabrication of hybrid coatings consisting of two steps: preparation of anodizing solution (step 1), fabrication of second coating (step 2).

Figure 2. SEM image of titania nanotubes at A) low magnification (4000X) and B) high magnification (16000X).

Figure 3. A) Current density-time transient registered for a sample anodized in glycerol/NaF electrolyte at 30 V. B) XRD pattern of the titania nanotubes after annealing treatments.

Figure 4. A) XRD pattern of 58S-BG powder. B) SEM image of 58S-BG-chitosan coating at two different magnifications (125X and inset: 500X). C) the EDS mapping of Ca, Si and P ions within the nanocomposite coating.

Figure 5. A) ATR-FTIR spectra of 58S-BG-chitosan with (SA-Blend) and without (SA-Less) sodium alginate. B) Water contact angle values of the pure titanium (Ti), 58S-BG-chitosan coated titanium (Ti/58S-BG-Chitosan), anodized titanium (TNT), anodized and chitosan coated titanium (TNT/Chitosan) as well as anodized and 58S-BG-chitosan coated titanium (TNT/58S-BG-Chitosan) (*$P < 0.05$).

Figure 6. SEM images of the A) Ti, B) Ti/58S-BG-Chitosan, C) TNT, D) TNT/Chitosan and E) TNT/58S-BG-Chitosan samples after soaking in SBF solution for 28 days. F) The pH value of SBF solutions during soaking of samples.

Figure 7. A) Antibacterial test against Gram-negative bacterium *E. coli* B) Antibacterial test against Gram-positive bacteria *S. aureus*. (*P < 0.05).

Figure 8. Scheme of three specimens, titania nanotube arrays (TNT), TNT coated with chitosan (TNT/Chitosan) and TNT coated with chitosan-Bioglass composite (TNT/58S-BG-Chitosan)

Figure 9. MG63 cell spreading on the various coatings; SEM images of MG63 cells after 7 days of culture on A) Ti, B) Ti/58S-BG-Chitosan, C) TNT, D) TNT/Chitosan and E) TNT/58S-BG-Chitosan coatings. Red arrows show the distribution and spreading of MG63 cells. F) Cell spreading, the fraction of area covered with cell clusters, on quintuple coatings. (*P < 0.05).

Figure 10. Cell viability of MG63 on various samples measured using MTT assays after 1, 3 and 7 days of culture. The absorbance was normalized against the control (TCP) at each time interval. (*P < 0.05).

Table 1- The average roughness (R_a), root mean square roughness (R_q), and maximum roughness depth (R_{max}) (mean ± SD) of the various samples determined by mechanical profilometer (*, **: compared to Ti and TNT, respectively) (*, **: P<0.05)

Name	$R_{a\ (nm)}$	$R_{q\ (nm)}$	$R_{max\ (nm)}$	Contact angle (°)
Ti	132 ± 26	147 ± 24	457 ± 133	72.5 ± 4.3
Ti/58S-BG-Chitosan	112 ± 19	98 ± 31	563 ± 170	76.4 ± 5.6
TNT	449 ± 15*	460 ± 16*	887 ± 214*	34.1 ± 5.5*
TNT/Chitosan	86 ± 3**	91 ± 12**	203± 87**	91.5± 6.3**
TNT/58S-BG-Chitosan	143 ± 41**	131 ± 21**	296 ± 149**	66.2 ± 2.9**

Figure

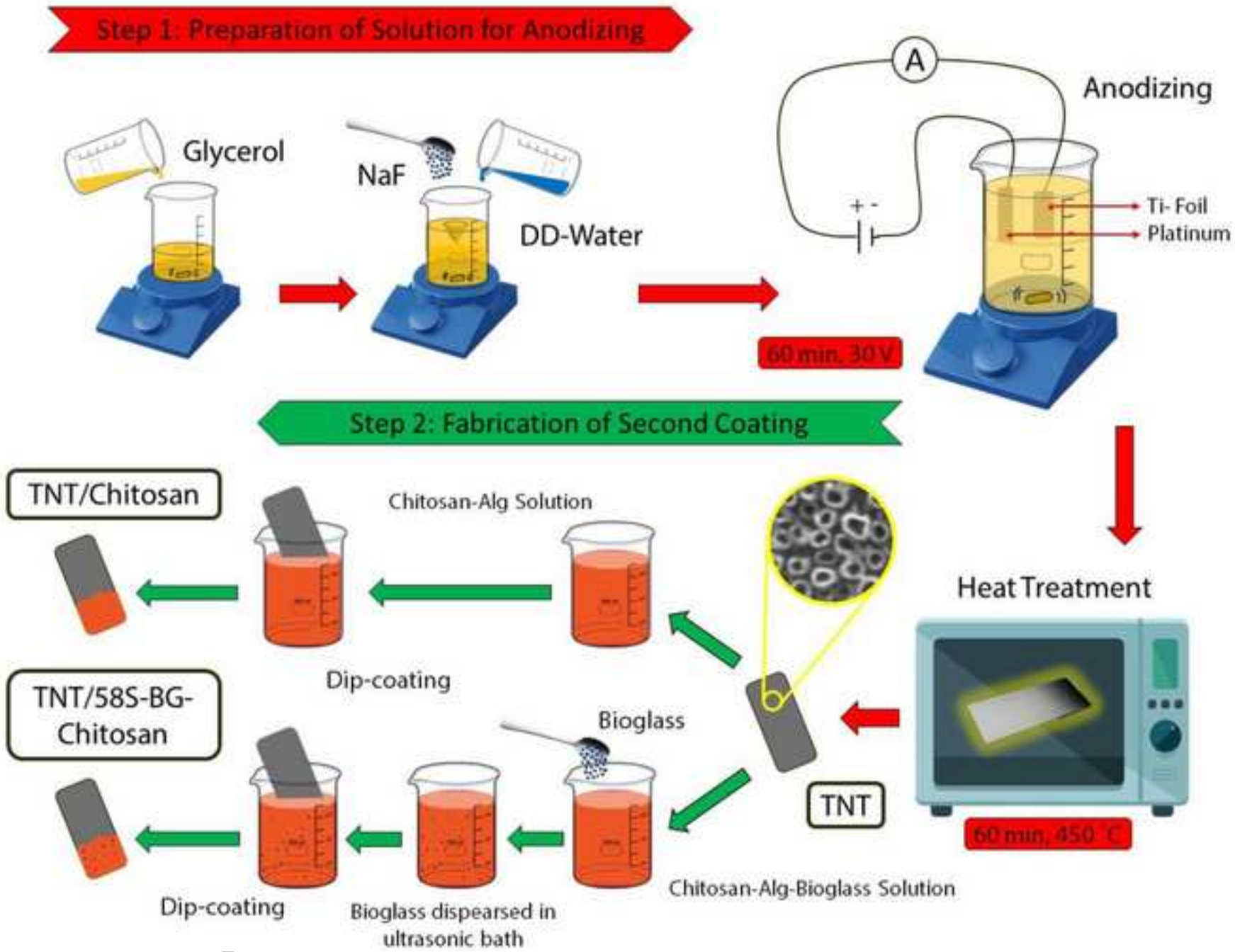

Figure

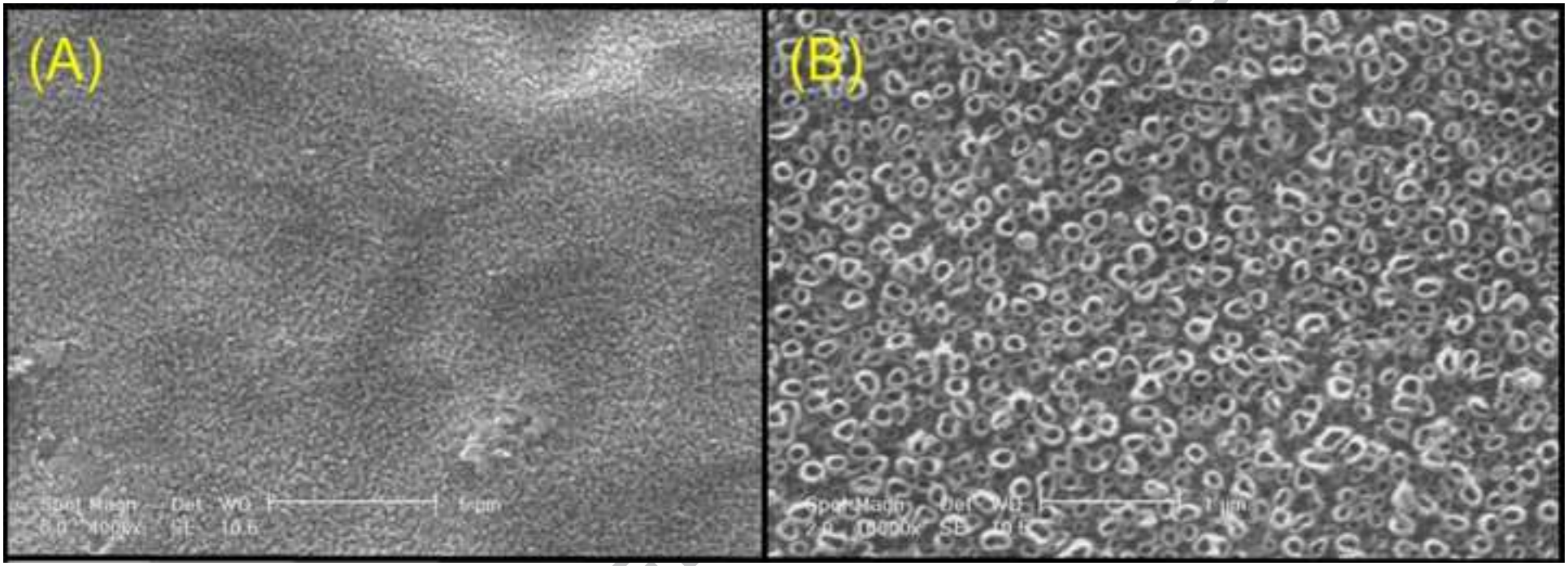

Figure

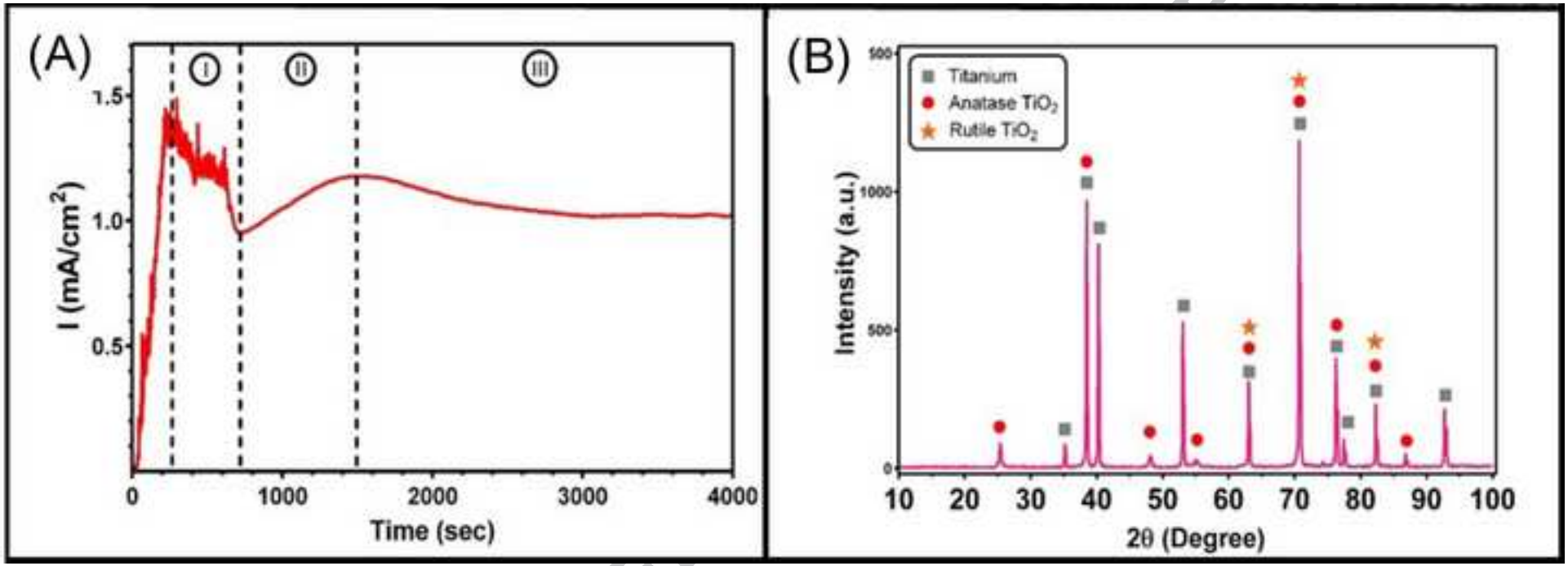

Figure

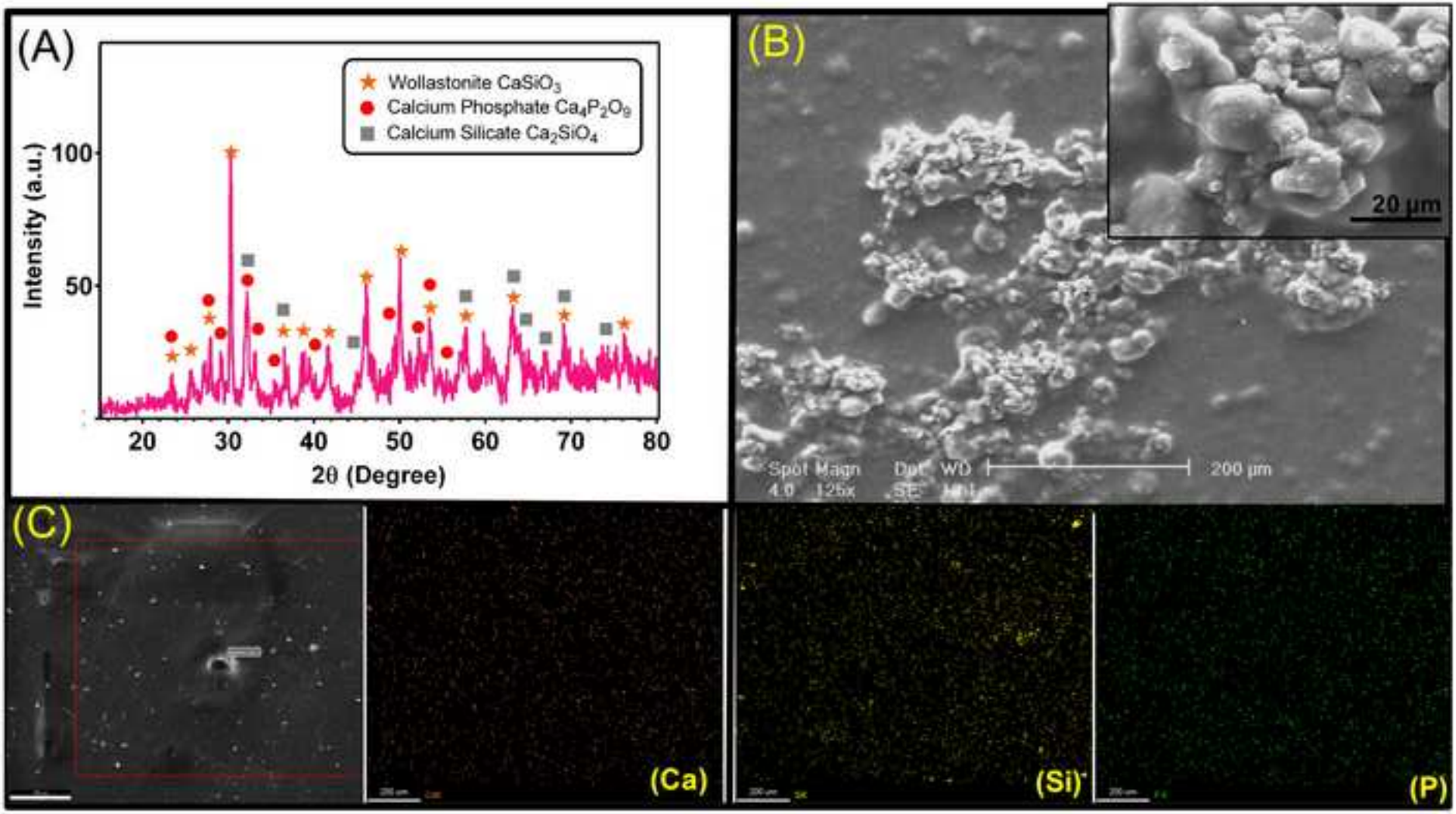

Figure

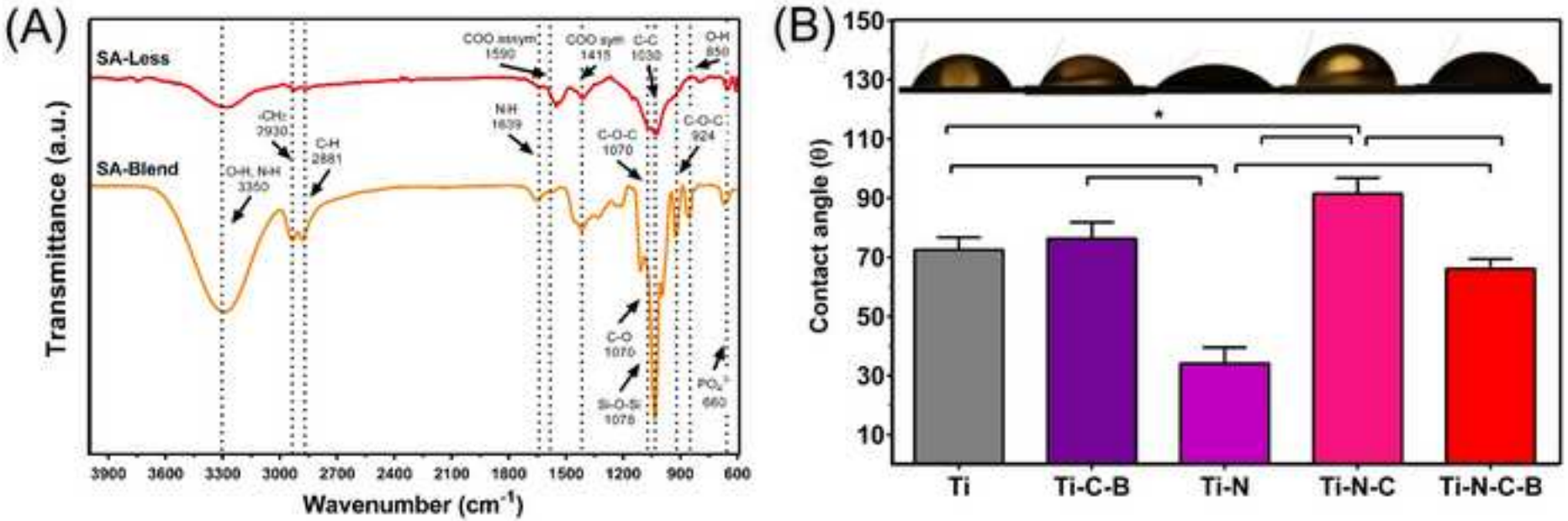

Figure

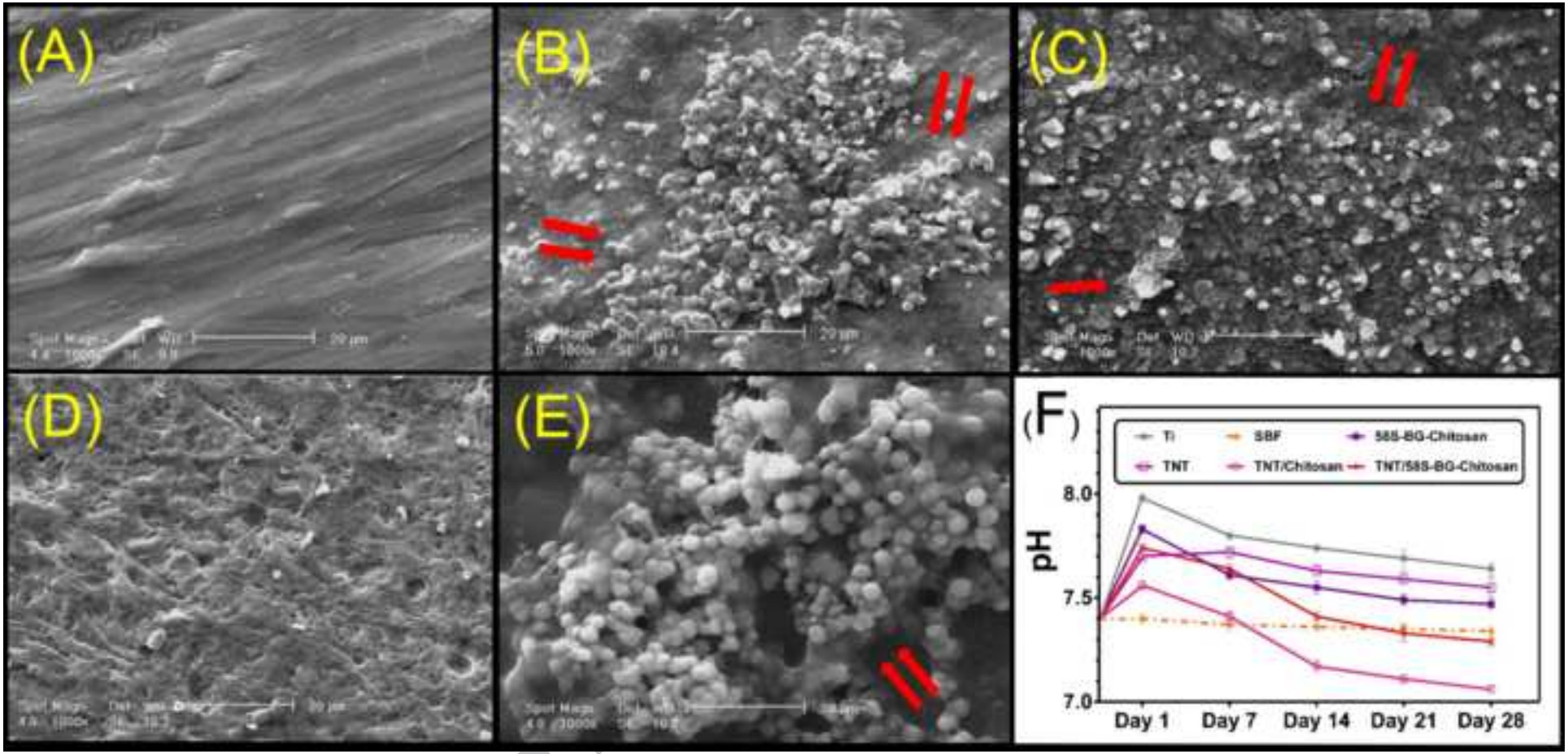

Figure

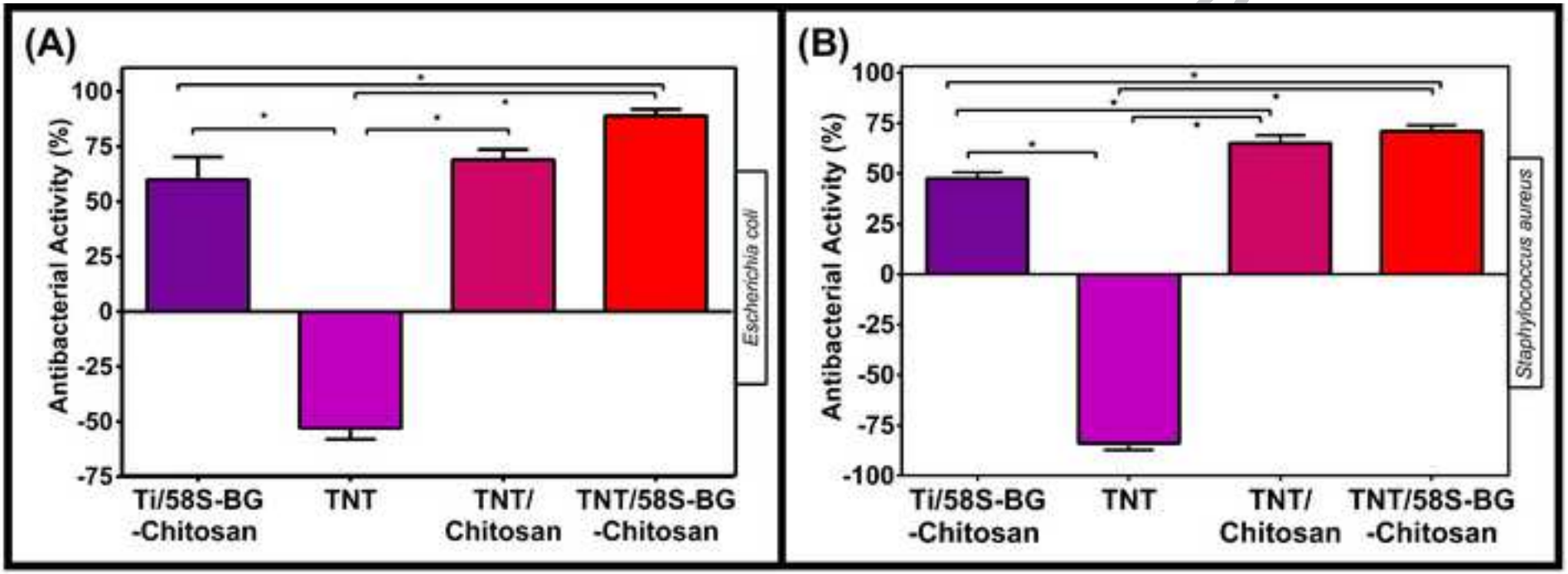

Figure

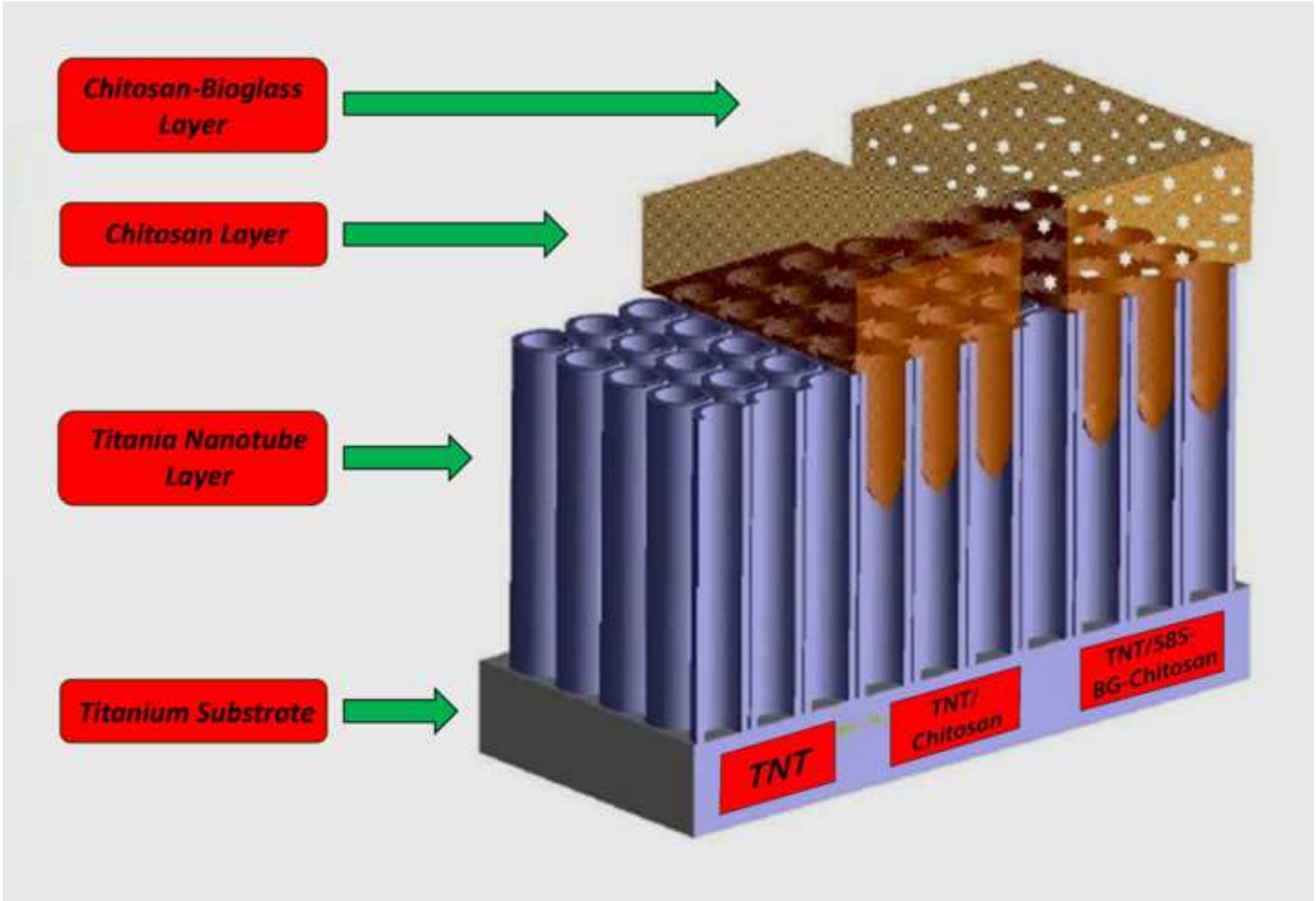

Figure

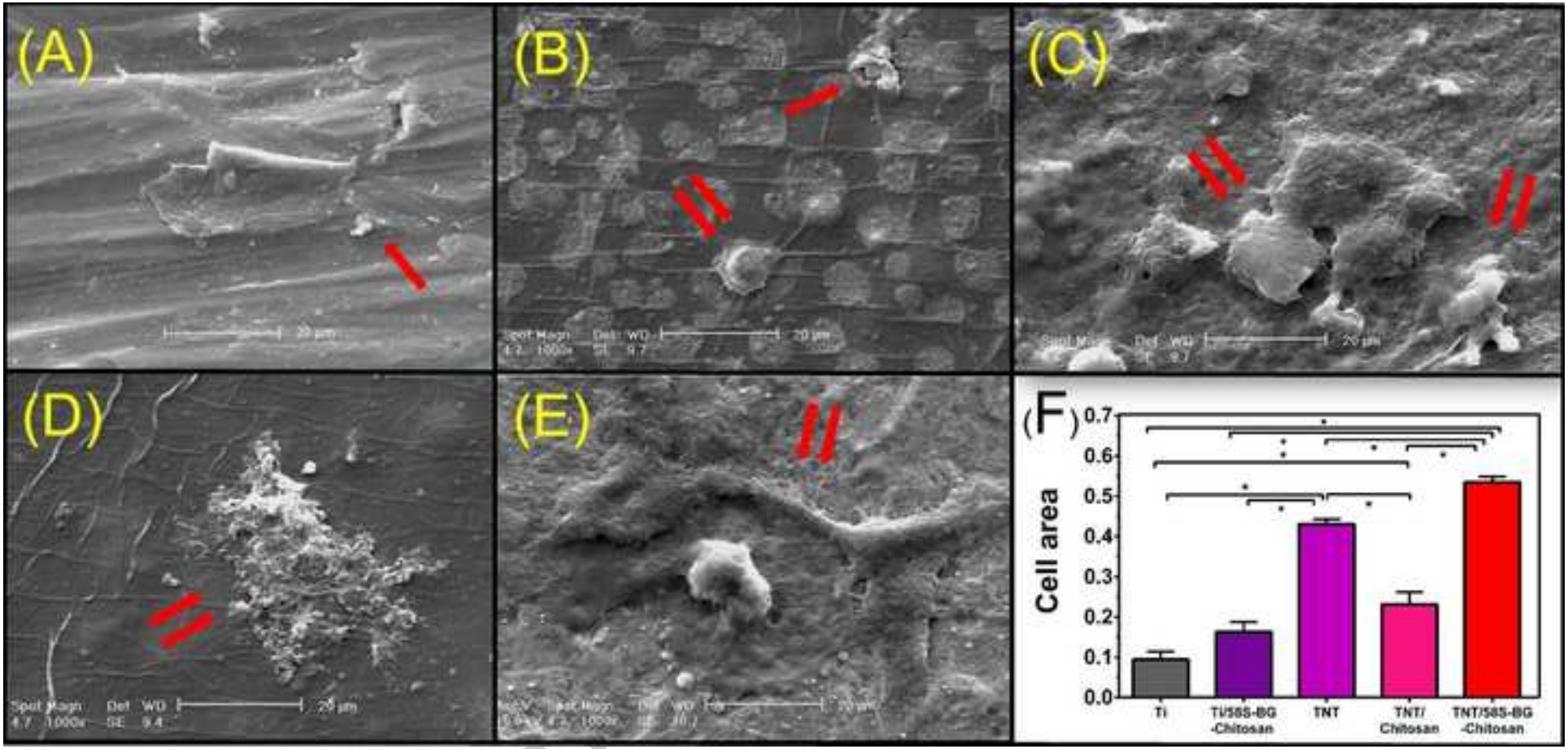

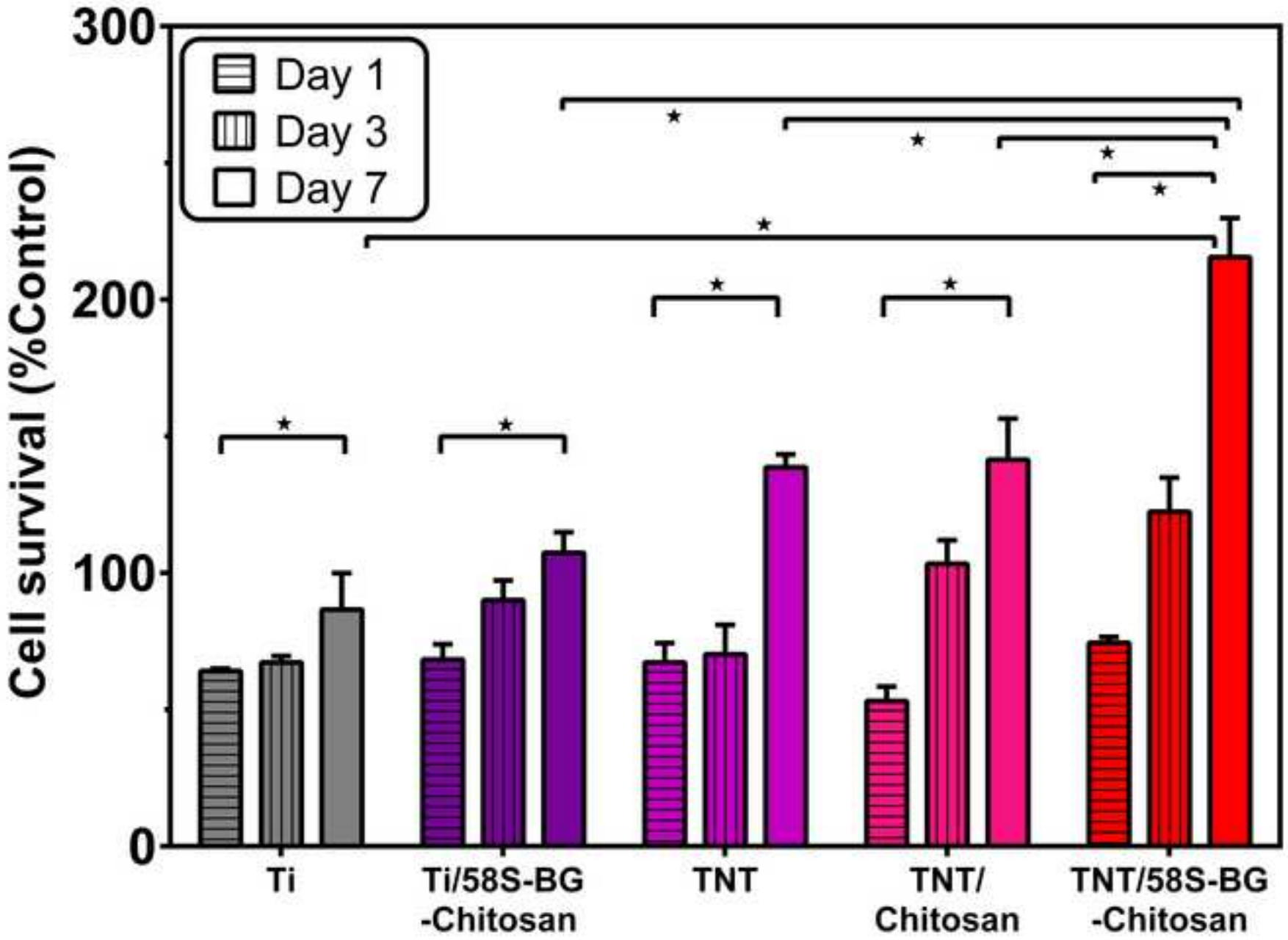

Graphical abstract

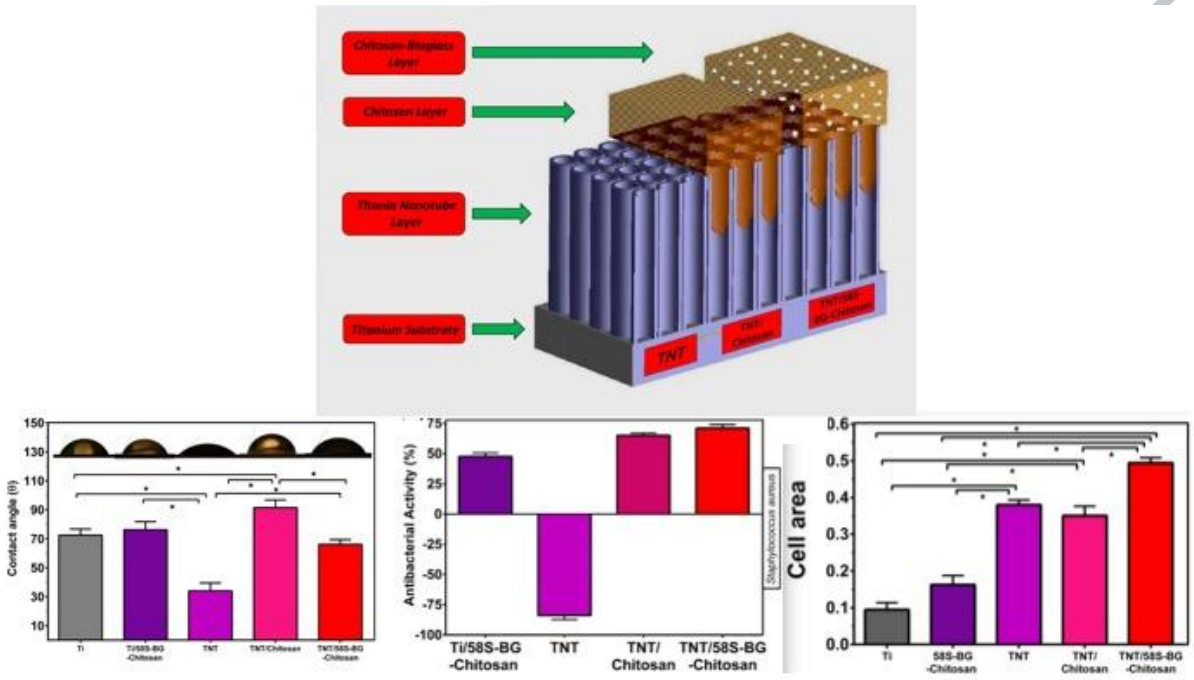

Highlight

- Two-layer titanium oxide nanotube (TNT)-chitosan/bioactive glass coating was developed
- TNT layer with inner diameter of 87 ± 15 nm was developed using anodization process
- TNT-chitosan/bioactive glass coating was superior in bone like apatite formation
- TNT-chitosan/bioactive glass coating has the highest antibacterial activity